Charge Scaling Force Field for Biologically Relevant Ions Utilizing a Global Optimization Method

Shujie Fan, Philip E. Mason, Victor Cruces Chamorro, Brennon L. Shanks, Hector Martinez-Seara,* and Pavel Jungwirth*

Institute of Organic Chemistry and Biochemistry, Academy of Sciences of the Czech Republic, Flemingovo nam. 2, CZ-16610 Prague 6, Czech Republic

E-mail: hseara@uochb.cas.cz; pavel.jungwirth@uochb.cas.cz

Abstract

Charge scaling, also denoted as the electronic continuum correction, has proven to be an efficient method of effectively including electronic polarization in force field molecular dynamics simulations without additional computational costs. However, scaling charges in existing force fields, fitted at least in part to experimental data, leads to inconsistencies such as overscaling. We have, therefore, recently developed a 4-site water model consistent with charge scaling, i.e., possessing the correct low-frequency dielectric constant of 45. Here, we build on top of this water charge scaled models of biologically relevant Li^+, Na^+, K^+, Ca^{2+}, Mg^{2+} cations and Cl^-, Br^-, and I^-, employing machine learning to streamline and speed-up the parameterization process. On the one hand, we show that the present model outperforms the best existing charge scaled model of aqueous ions. On the other hand, the present work points to a future need for improving consistently and simultaneously the water and ion models within the electronic continuum correction framework.

Introduction

Effective inclusion of electronic polarization by charge scaling has been shown to improve the description of interactions of ions in aqueous environments without additional computational costs.[1–4] This so called electronic continuum correction (ECC) can, in particular, fix overbinding pertinent to high charge density ions like lithium, calcium, magnesium, and others described by standard non-polarizable force fields.[5–8] While this correction is well physically justified – it is equivalent to immersing the system into a dielectric continuum with the high-frequency dielectric constant (of about 1.78 for water) – one has to be careful not to overscale. Namely, existing non-polarizable water models have been parameterized against experiment and, as a result have dielectric constants higher than what would correspond purely to the dielectric response of the nuclei.[9–11] In other words, (part of) the high-frequency electronic response has been translated in an uncontrolled way to the low-frequency nuclear rearrangements. In order to avoid potential artifacts connected with grafting charge scaling on top of such water models we have recently parameterized a *de novo* 4-site water model better compatible with the ECC approach, i.e., possessing a dielectric constant of 45, corresponding to the genuine nuclear response only.[12] We have shown that despite its low dielectric constant, this model, denoted as ECCw2024, performs as well as the best existing 4-site water models, such as TIP4P/2005.[11,12]

In this work, we move a step further in developing from scratch a charge-scaled force field for biomolecular simulations that is compatible from the onset with the ECC concept. Using machine learning techniques to save computer time during parameterization, we build parameters for the following biologically relevant ions – Li^+, Na^+, K^+, Ca^{2+}, Mg^{2+}, Cl^-, Br^-, and I^-. By obtaining better agreement with the experimental structural, thermodynamic and especially dynamic properties for the corresponding salt solutions than for the hitherto best model of this type,[13] we demonstrate that our systematic approach to developing charge-scaled force fields pays off. Also, while these ion models are built upon ECCw2024 water, we show that they perform rather well also with TIP4P/2005, demonstrating the robustness

of our approach. Finally, by optimizing the scaling parameter within physically justified margins, we open the path to further improving charge-scaled force fields.

Methods

Optimization process

An automated framework was utilized for the optimization process that was originally developed for parameter sampling of the ECC water model.[12] A random walk algorithm was first applied to generate 200 parameter sets, with initial values taken from the prosECCo75 force field.[14] Following this initial sampling, a differential evolution (DE) algorithm was used to refine the parameters and achieve an optimized dataset.

Each sample was evaluated using a negative log-likelihood cost function defined as:

$$J(\boldsymbol{\theta}) = \sum_{i=1}^{n} \left[\frac{n}{2} \log(2\pi\sigma_i^2) + \frac{1}{2\sigma_i^2} (y_i(\boldsymbol{\theta}) - \mu_i)^2 \right] \tag{1}$$

where $\boldsymbol{\theta}$ denotes the the parameter set, y_i represents the target property calculated from MD simulations, μ_i is denotes the corresponding reference experimental value, σ_i is the predefined sample variance. In practice, all target properties were included during the optimization to achieve a globally optimized parameter set that performed well across multiple properties, rather than excelling at reproducing a single property.

To efficiently explore the parameter space while avoiding regions where predicted properties deviate significantly from experimental references, we integrated a local Gaussian process (LGP) model[15] with the differential evolution algorithm. DE is a population-based global optimization method that evolves a set of candidate solutions (parameter vectors) through mutation, crossover, and selection. In each generation, new candidate parameter sets (offspring, denoted $\boldsymbol{\theta}$) are generated by perturbing existing ones (parents, denoted $\boldsymbol{\theta'}$), and a selection step determines whether the offspring should replace its parent.

To accelerate the evaluation of new parameter sets, the LGP model was used to predict physical properties directly, bypassing the need for full molecular dynamics (MD) simulations. The LGP model was initially trained on data generated by a random-walker algorithm, using force field parameters as input and corresponding target physical properties as output. As the optimization progressed, the LGP model was retrained after every 50 new data points, using the entire dataset collected so far, including both existing and newly added examples. This active learning scheme ensured that the model continuously adapted to the expanding and increasingly diverse data space.

In practice, consider for example a parent parameter set $\boldsymbol{\theta'}$ that has already been evaluated through MD simulation, resulting in a cost function value $J(\boldsymbol{\theta'})$. A new offspring parameter set $\boldsymbol{\theta}$ is generated by applying DE's mutation and crossover steps to $\boldsymbol{\theta'}$. Before committing computational resources to simulate $\boldsymbol{\theta}$, the LGP model estimates the physical properties and computes a predicted cost $J(\boldsymbol{\theta})$. The selection of whether to accept $\boldsymbol{\theta}$ is determined by the Metropolis-Hastings criterion:

$$A(\boldsymbol{\theta}, \boldsymbol{\theta'}) = min\left(1, e^{J(\boldsymbol{\theta'})-J(\boldsymbol{\theta})}\right) \tag{2}$$

A random number $u \in [0, 1]$ is drawn, and if $u \leq A(\boldsymbol{\theta}, \boldsymbol{\theta'})$, the offspring $\boldsymbol{\theta}$ is accepted for MD simulation and added to the training dataset; otherwise, it is rejected and discarded.

The parameters of the atomic ions were optimized against the target values, including structural information from neutron scattering, thermodynamic properties (e.g. density), and kinetic properties such as viscosity. Diffusion coefficients of water oxygen in the solutions were also used for further validation. The atomic ions were divided into two groups based on the methods used to measure the structure of aqueous solutions. The first group, Li^+, K^+, Ca^{2+} and Cl^-, was measured in solutions of 3m LiCl,[6] 6m LiCl,[16] 4m KCl,[17] and 4m $CaCl_2$[18] using neutron diffraction experiments with isotopic substitution (NDIS). This method enables the estimation of partial structure factors from the total structure factor by

assuming that solutions with identical chemical compositions, but different isotopic concentrations, are structurally equivalent. The second group, consisting of Na^+, Mg^{2+}, Br^-, and I^-, was measured in 4m NaCl,[19] 3m $MgCl_2$,[7] 4m KBr, and 4m KI solutions using a 'null' water mixture technique.[20] The ions in the first group were optimized before those in the second group, as NDIS provides more detailed insights into ion-solution correlations.

The optimized parameters included the scaling factor and Lennard-Jones (LJ) ϵ and σ values for cations and anions, following the Lorentz-Berthelot combination rules:

$$\sigma_{ij} = \frac{\sigma_{ii} + \sigma_{jj}}{2}, \epsilon_{ij} = \sqrt{\epsilon_{ii}\epsilon_{jj}}. \tag{3}$$

Furthermore, we included pair-specific LJ ϵ and σ between anions and water oxygen atoms, as they improved the physical qualities of the ionic solutions. However, not all possible pairwise parameters (i.e., cation-anion, cation-oxygen, anion-oxygen, and self-self interactions) were explicitly included. This decision was based on two key considerations: 1. For the ionic solutions studied here, cation–cation and anion–anion LJ interactions have minimal impact on the target properties. Therefore, the meaningful interactions are primarily cation-anion, cation-oxygen, and anion-oxygen, and the degree of freedom of the parameters of these are 6 (3×2), where the 2 corresponds to ϵ and σ). This is equivalent to the degrees of freedom when considering only the combination-rule ϵ and σ for cations, anions, and anion-oxygen pairs. 2. Including all pairwise interactions would significantly increase the dimensionality of the parameter space, resulting in higher computational costs for achieving convergence and generating sufficient samples to train the LGP model.

The parameters were initially sampled independently for each solution to explore the optimal model when there were no restrictions on neither the scaling factor nor the Cl^- model, which ultimately should be shared between salt pairs. During this procedure, each solution, such as LiCl, $CaCl_2$ and KCl, was thus allowed to have different optimal scaling factors and Cl^- parameters. These separately optimized parameters served as training data

for the LGP model and provided an insight into the optimal behavior of ion models in a specific solution which would help us determine whether it would be necessary to add cation-anion pairwise parameters during the final optimization. Then the Li^+, Ca2+, K^+, and Cl^- parameters were refined jointly, ensuring consistent Cl^- parameters and a shared scaling factor across all systems. We followed by optimizing Na^+, Mg^{2+}, Br^-, and I^- using the established optimal scaling factor and Cl^- parameters. I^- and Br^- were refined using a fixed scaling factor and the optimized K^+ parameters from the previous stage, aiming to reproduce experimental behavior in 4m KI and KBr solutions. Similarly, Na^+ and Mg^{2+} were optimized using the refined Cl^- model, with experimental data from 4m NaCl and 3m $MgCl_2$ solutions as reference. The optimization by stages was needed due to the differences in structural data (i.e., neutron scattering data) available for the salt solutions.

Simulation Details

Molecular dynamics simulations were performed for all accepted parameters to estimate target properties, using the GROMACS 2022 molecular dynamics package.[21] The simulated cubic box contained 2776 ECCw2024 water molecules along with cations and anions, whose numbers were adjusted to achieve the target electrolyte concentration. Each system underwent energy minimization followed by a 7 ns isothermal-isobaric (NPT) simulation. The NPT simulations were performed under periodic boundary conditions at a constant temperature (300 K for optimization and 298 K for validation) and pressure (1 bar). Temperature control was achieved using the Nosé–Hoover thermostat[22] with a time constant of 1 ps, while an isotropic pressure coupling scheme was applied using the Parrinello-Rahman barostat,[23] with a compressibility of 5×10^{-5} bar^{-1} and a time constant of 5.0 ps. Long-range electrostatics and long-range Lennard-Jones potentials were calculated with the smooth particle mesh Ewald method[24] with an initial cutoff of 1.2 nm. Interactions beyond the cutoff were calculated in reciprocal space with a fast-Fourier transform on a grid with an initial spacing of 0.10 nm and fourth-order spline interpolation.

Radial distribution functions (RDFs) and densities were calculated from the last 6 ns of the NPT simulation, with the initial 1 ns excluded for equilibration. The RDFs were calculated as

$$g_{\alpha\beta}(r) = (N_\alpha N_\beta)^{-1} \sum_{i=1}^{N_\alpha} \sum_{j=1}^{N_\beta} \langle \delta(|\mathbf{r}_i - \mathbf{r}_j| - r) \rangle \tag{4}$$

where N_α and N_β are the total number of atom type α and atom type β, respectively. The calculated RDFs were compared with neutron scattering results, with additional details provided in the Supporting Information. To evaluate ion pairing in the first hydration shell of cations, the number of contact ion pairs (CIPs) was calculated from the cation-anion RDF as:

$$n^{CIP} = 4\pi\rho_{+/-}(r) \int_0^{r_{min}} g_{+-}(r) r^2 dr \tag{5}$$

where $g_{+-}(r)$ is the RDF between cations and anions, and $\rho_{+/-}$ is the number density of cations or anions. The upper limit of the integral, r_{min}, corresponds to the position of the first minimum in $g_{+-}(r)$. If no distinct peak is observed in $g_{+-}(r)$ within the first hydration shell, which is defined based on the ion-water RDF, n^{CIP} is considered to be zero. The coordination number (CN), representing the total number of atoms (water oxygen or counterions) in the first hydration shell, was computed as:

$$n^{CN} = n^{CIP} + 4\pi\rho_{\mathrm{H_2O}}(r) \int_0^{r_{min}^{MO}} g_{MO}(r) r^2 dr \tag{6}$$

where g_{MO} is the ion-oxygen RDF, $\rho_{\mathrm{H_2O}}$ is the number density of water molecules, and r_{min} corresponds to the first minimum in g_{MO}.

The final frame from the NPT simulation was used as the starting structure for three independent 2 ns non-equilibrium simulations with a cosine acceleration to calculate viscosity.[25] The settings were identical to those of the NPT simulations, except that pressure coupling was disabled, and a cosine acceleration amplitude of 0.020 nm/ps^2 was applied.

To further evaluate the optimized models, additional simulations were performed with

the optimal parameters. Equilibrium and non-equilibrium simulations were conducted for all salt solutions at concentrations of 0.24 m, 1 m, 3 m, and 4 m, with the same settings as those used during the optimization process. For LiCl, an additional concentration of 6 m was included. To ensure accurate estimates of means and standard deviations, 25 independent 2 ns non-equilibrium simulations with cosine acceleration were conducted for viscosity calculations. Similarly, 25 independent 2 ns NVT equilibrium simulations were performed to calculate the diffusion coefficient of water oxygen atoms in each solution.[26] These NVT simulations followed the same settings as the NPT simulations, except that pressure coupling was disabled. The diffusion coefficient was calculated using the Einstein approach:

$$D = \lim_{t\to\infty} \frac{d}{dt} \left\langle \frac{1}{6N} \sum_{i=1}^{N} |r_i(t) - r_i(0)|^2 \right\rangle \tag{7}$$

where $r_i(t)$ and $r_i(0)$ represent the position of the i-th particle at time t and a reference time t=0, respectively, and N is the total number of the particles in the system. A finite-size correction was applied according to the method proposed by Yeh and Hummer:[27]

$$D_\infty = D(L) + \frac{k_\mathrm{B} T \xi}{6\pi\eta L} \tag{8}$$

where D_∞ is the infinite system size self-diffusion coefficient, $D(L)$ is the self-diffusion coefficient calculated for a cubic box with edge length L, η is the shear viscosity obtained from the cosine acceleration non-equilibrium simulations, and = 2.837298 is a dimensionless constant. It's important to note that this correction term incorporates simulation-derived parameters, which may introduce additional sources of error in estimating D_∞. To assess this potential error, we compared the correction calculated using the edge length and shear viscosity of an ideal solution box, matching experimental density and viscosity values, and found that the additional error introduced by the simulation-derived L and η in the correction term was less than 2%. Therefore, we have included the corrected results in our analysis.

We repeated the simulations for our optimal models using the TIP4P2005 water model

to test the transferability of our parameters to other water models. Additionally, simulations were carried out for the Madrid2019 ion models with both ECCw2024 and TIP4P2005 water models as references for comparison.

Results and discussion

Optimization of a ECC compatible ion force field

Building on the recently developed ECCw2024 water model, we now turn to the development of a ECC-compatible force field for ions. In this work, we systematically optimize the charge scaling factor and the Lennard-Jones (LJ) parameters σ and ϵ for a set of biologically and technologically relevant ions, namely, the Li^+, Na^+, K^+, Ca^{2+}, and Mg^{2+} cations and the Cl^-, Br^-, and I^- anions. To enhance the transferability of the resulting force field, we prioritize the use of combination rules over the inclusion of ion-specific pair interactions. Specific pair parameters are incorporated only when they yield clear and significant improvements in accuracy.

Our optimization method targeting thermodynamic, dynamic, and structural properties yielded a plethora of acceptable models, representing a sizable convex hull in the parameter space. Figure 1 shows the distribution of scaling factors for all accepted samples during the optimization. These acceptable models exhibit scaling factors ranging from 0.7 to 0.9. The top-performing models have scaling factors between 0.78 and 0.83, indicating that good models are abundant within this range when optimized with our ECCw2024 water model. The scaling factor 0.81 emerged as both the optimal and the most populated one among the top 25 models ranked by the cost function.

The fact that the optimal scaling factor of 0.81 is somewhat higher than the value of 0.75 following from the high-frequency dielectric constant of water is consistent with our recent finding of a slightly attenuated dielectric screening pertinent to closely interacting ions.[28] Indeed, our optimization cost function incorporates neutron diffraction with isotopic

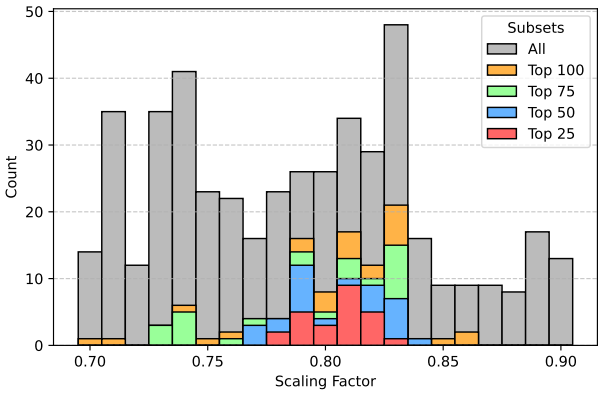

Figure 1: Distribution of scaling factors for the top 25, 50, 75, 100, and all samples from the final optimization stage of ions including Li^+, Na^+, K^+, Ca^{2+} and Cl^-.

substitution data (i.e., first order difference of real-space signals), which primarily reflect the first and second hydration shells of solvated ions. Our optimal scaling factor also aligns closely with a recently developed scaled-charge potassium model with a scaling factor of 0.78, which shows excellent agreement with experimental conductivity data critical to simulate potassium channels.[29]

The set of parameters for the best-performing model, denoted as ECCions81, is presented in Table 1. It is of interest to compare these parameters with those of the Madrid2019 force field,[13] probably the best-performing charge scaling ion models to date. Besides the difference in scaling factors (0.85 for Madrid2019), a notable distinction between the ECCions81 model and Madrid2019 lies in the resulting LJ parameters of our ions in water (Table S3). Cations in our ECCions81 model have systematically larger LJ σ values compared to Madrid2019, with an average increase of 0.17 Å for monovalent cations and 0.38 Å for divalent cations, reflecting a larger effective ionic radius in water. In contrast, our ECCions81 anions exhibit smaller σ values compared to Madrid2019, with an average reduction of 0.5 Å. Additionally, the difference between cation-oxygen and cation-anion σ values is significantly smaller in our ECCions81 model than in Madrid2019.

These differences lead to a greater tendency for contact ion pairing within the first hydration shell in the ECCions81 model, while the overall coordination number remains nearly

Table 1: Parameters of the ECCion81 Force Field. Charges and Lennard-Jones σ, ϵ parameters for electrolyte solutions in ECCw2024 water, including Li^+, Na^+, K^+, Mg^{2+}, Ca^{2+}, Cl^-, Br^-, and I^-. Since the pairwise Lennard-Jones parameters between water oxygen and cations follow the Lorentz-Berthelot combination rules, the parameters for ECCw2024 oxygen are also listed. For anions, specific anion-oxygen pairwise Lennard-Jones parameters are provided.

Charges (e)					
$q_{Li} = q_{Na} = q_K = 0.81$, $q_{Mg} = q_{Ca} = 1.62$, $q_{Cl} = q_{Br} = q_I = -0.81$					
Ion	**σ (nm)**	**ϵ (kJ/mol)**	**Ion**	**σ (nm)**	**ϵ (kJ/mol)**
Li^+	0.151568	0.217304	Cl^-	0.393492	0.714723
Na^+	0.237287	0.154682	Cl-O	0.352611	0.723797
K^+	0.297000	0.844526	Br^-	0.441421	1.515692
Mg^{2+}	0.123364	4.504426	Br-O	0.360099	1.172294
Ca^{2+}	0.240765	0.900759	I^-	0.476172	1.295655
O [12]	0.315480	0.761154	I-O	0.372802	0.921039

unchanged compared to Madrid2019 (Table 2). This increase in contact ion pairing affects radial distribution functions and significantly influences transport and dynamic properties of the solutions, which are explored in detail in the following sections.

Table 2: Comparison of CIP and CN values for ECC and Madrid2019 across different salt solutions.

Solution	**ECCions81**		**Madrid2019**	
	CIP	CN	CIP	CN
6m LiCl	0.43	4.03	0	3.99
3m LiCl	0.22	4.01	0	4.00
3m $MgCl_2$	0.72	6.05	0	6.01
4m $CaCl_2$	1.04	6.35	0.01	7.31
4m KCl	0.83	6.85	0.35	6.72
4m NaCl	0.59	5.35	0.04	5.43
4m KBr	0.91	6.94	0.08	6.58
4m KI	0.52	6.90	0	6.31

Densities and dynamic properties

Our ECCions81 ions model demonstrates excellent agreement with experimental density values, with deviations typically below 0.5%, comparable to the performance of Madrid2019 (Figure 2 and Table S4). This high level of accuracy is consistently observed across most

tested solutions, including LiCl, NaCl, KI, and $MgCl_2$, where both models align closely with experimental measurements. In KCl and KBr solutions, ECCions81 slightly underestimates the density by approximately 0.7%, equivalent to a difference of 10 kg/m^3. A more notable deviation occurs in $CaCl_2$ solutions, where the ECCions81 model underestimates the density by 3.5% at 4 M, corresponding to a difference of 50 kg/m^3 from experimental values. Note that Madrid2019 accurately reproduces the experimental densities for these solutions.

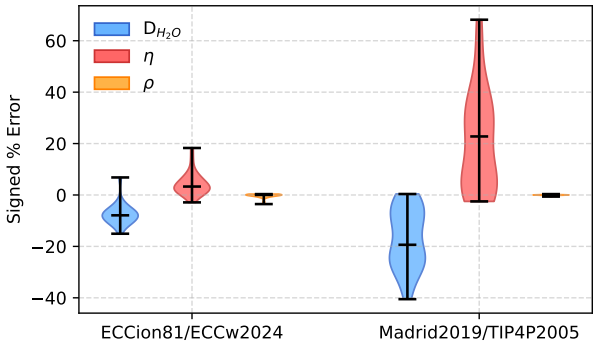

Figure 2: Signed percentage errors in the self-diffusion coefficient of water (D_{H_2O}), viscosity (η), and density (ρ) predicted from simulations using two water-ion models: ECCion81/ECCw2024 and Madrid2019/TIP4P2005, with experimental data as the reference. Violin plots represent the distribution of errors across all tested electrolyte solutions at various concentrations. Horizontal bars indicate the medians, and the full range of data is shown to highlight variability and systematic deviations.

The ECCions81 model outperforms Madrid2019 in reproducing the concentration dependence of both viscosity and water self-diffusion coefficients (D_{OW}) across all tested electrolyte solutions (Figure 2 and Tables S5 and S6). Viscosity deviations in ECCions81 generally remain below 10%, while Madrid2019 frequently overestimates viscosity by more than 25% at high concentrations. The discrepancy is particularly severe for $MgCl_2$, where Madrid2019 deviates by over 60% at 4 m, in contrast to ECCions81, which closely matches the experimental data. In LiCl solutions, ECCions81 shows somewhat higher deviations in viscosity (up to 16% at 6 m), yet still significantly improves on Madrid2019, which deviates by 64%. For KCl, KBr, and KI, where viscosity changes only weakly with concentration, the ECCions81 model accurately captures the trend with deviations below 10%, whereas Madrid2019 overshoots

by more than 30%. Despite not being an explicit optimization target, we observe similar trends for water diffusion (D_{OW}). Namely, ECCions81 maintains deviations within 10% for most salts, while Madrid2019 underestimates water mobility, with errors reaching as much as 40%. Again, 6 m LiCl is the most extreme case, with deviations of 15% for ECCions81 and 41% for Madrid2019. ECCions81 also better captures the weak concentration dependence of D_{OW} in KCl, KBr, and KI solutions, whereas Madrid2019 consistently overestimates the effect of salt concentration for dynamic properties.

Comparisons to neutron scattering data

This section compares the simulation results of the first-order difference functions in r-space and Q-space for Cl^- with neutron diffraction data (i.e., NDIS experiments). While both representations contain the same information, they emphasize different aspects: Q-space highlights peak positions related to phasing, whereas r-space facilitates the interpretation of peak heights and the overall understanding of the molecular surroundings of the ions.

Overall, we see that ECCions81 systematically matches better experimental peak heights in r-space and phases in Q-space, with Madrid2019 consistently overestimating peak intensities in r-space. ECCions81 also improves the peak positions for Br^- and I^- and significantly reduces the artificial O–O peak at 2.8 Å (Figures S15 and S17). These improvements stem from moderate ion pairing in ECCions81, which weakens ion-water correlations.

Below, we focus on detailed comparisons between the simulation results and neutron diffraction experiments. We discuss primarily first-order difference functions (both in real and reciprocal spaces) where we possess high quality experimental data for Li^+, K^+, Ca^{2+}, and Cl^-. Less direct neutron diffraction data are available to us for Mg^{2+}, Br^-, I^- and Na^+ ions, as discussed briefly below and further in the Supporting Information.

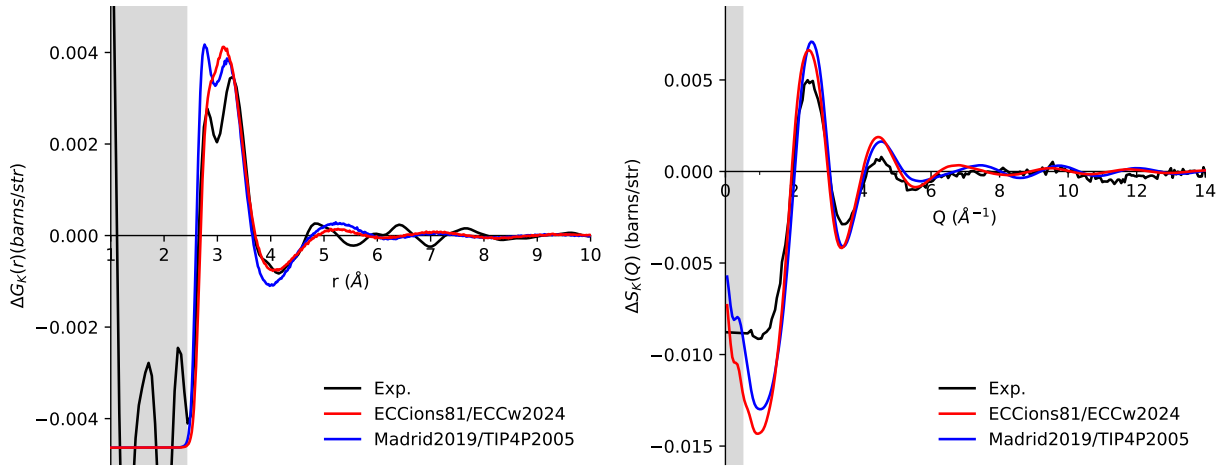

Figure 3: First-order difference functions $\Delta G_K(r)$ (left) and $\Delta S_K(Q)$ (right) for simulations of 4m KCl solution using the ECCions81 model with the ECCw2024 water model (red) and the Madrid2019 ion model with the TIP4P/2005 water model (blue), and experimental data (black). Gray shading indicates regions where the experimental signal consists of only noise (in r-space) or falls outside the measurement range (in Q-space).

Potassium

Monovalent ions, particularly the relatively large K^+ ions that exhibit low charge density, are generally considered straightforward to model. In principle, their weakly bound coordination shells should not pose a major challenge for classical force fields and charge scaling is expected to play only a minor role in accurately capturing their solvation behavior. The comparison between simulation results and NDIS results for 4m KCl solution is shown in Figure 3. In r-space, Madrid2019 captures the successive dual peaks between 2.8–3.8 Å, but significantly overestimates the height of the first peak, corresponding to the K-O correlation (Figure S7). In contrast, ECCions81 produces a single peak rather than dual peaks with similar overshooting intensity as the Madrid model, while the first minimum fits the experimental data perfectly. Beyond this minimum, the apparent match with the experimental data is reduced with a significant diphase. In Q-space, both models exhibit a similar structure, characterized by higher first and second peaks, deeper minima between these peaks, and a reduced signal in the low-Q region compared to experimental values. While the low-Q signal for Madrid2019 is slightly higher than that of ECCions81, both models deviate from

experimental data in this region.

A more detailed comparison of K^+ simulation results with experimental data is provided in the Supporting Information, including a reference model that shows better agreement with the r-space data but yields a less accurate density. Overall, despite the anticipated simplicity of the description of potassium ions none of the existing models fit perfectly the experimental data. Still, ECCions81 improves structural agreement compared to Madrid2019, while maintaining reasonable density predictions.

Calcium

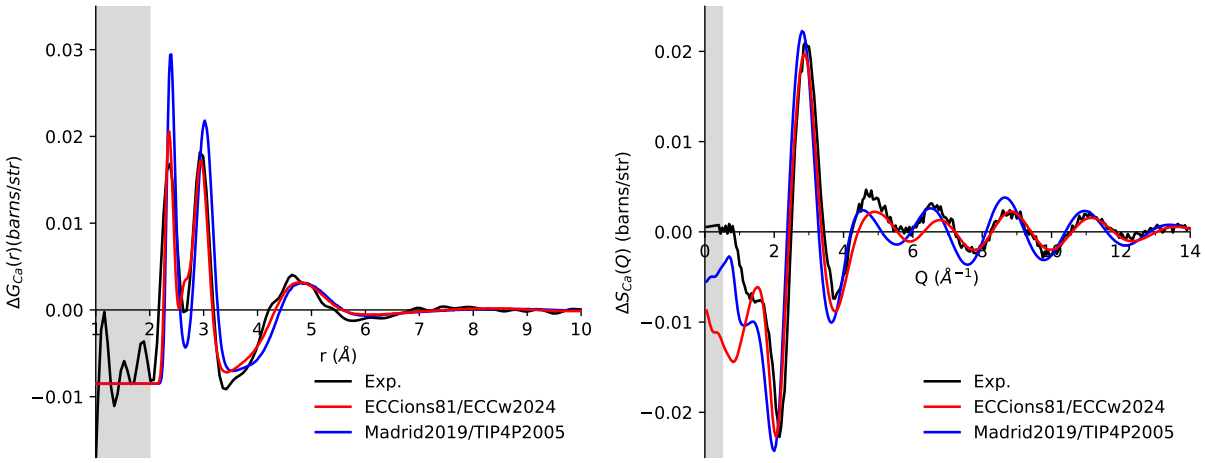

Figure 4: First-order difference functions $\Delta G_{Ca}(r)$ (left) and $\Delta S_{Ca}(Q)$ (right) for simulations of 4m $CaCl_2$ solution using the ECCions81 model with the ECCw2024 water model (red) and the Madrid2019 ion model with the TIP4P/2005 water model (blue), and experimental data (black). Gray shading indicates regions where the experimental signal consists of only noise (in r-space) or falls outside the measurement range (in Q-space).

Divalent cations with high-density charges are known to be harder to model, with charge scaling playing a more relevant role.[4] First-order difference functions of Ca^{2+} in a 4m $CaCl_2$ solution in both r-space and Q-space were calculated and compared with experimental data, with the results shown in Figure 4. In r-space, both ECCions81 and Madrid2019 models capture the two prominent peaks at approximately 2.3 Å and 3.0 Å, as well as the third minor peak at around 4.8 Å. The first two peaks correspond to the Ca-O and Ca-H correlations in

the first hydration shell. In contrast, the third peak arises from a combination of Ca-O, Ca-H, and Ca-Cl correlations in the second hydration shell, as shown in Figure S6. The stronger Ca-Cl pairing in ECCions81 reduces the correlations between Ca and water, introduces a small bump at the local minimum at around 2.6 Å, and lowers the height of the first and second peaks, bringing them closer to experimental values. In contrast, the Madrid2019 model does not exhibit any Ca-Cl pairing.

In Q-space, ECCions81 shows better overall agreement with experimental data than Madrid2019 across the full Q-range, particularly in capturing signal amplitudes. Madrid2019 exhibits slightly better phase agreement around 1 $Å^{-1}$—a region corresponding to long-range structural correlations in r-space—which may be related to its improved performance in reproducing bulk density. It also shows improved phase alignment in the 4–7 $Å^{-1}$ range, although the associated structural features in r-space are less clearly defined.

Lithium

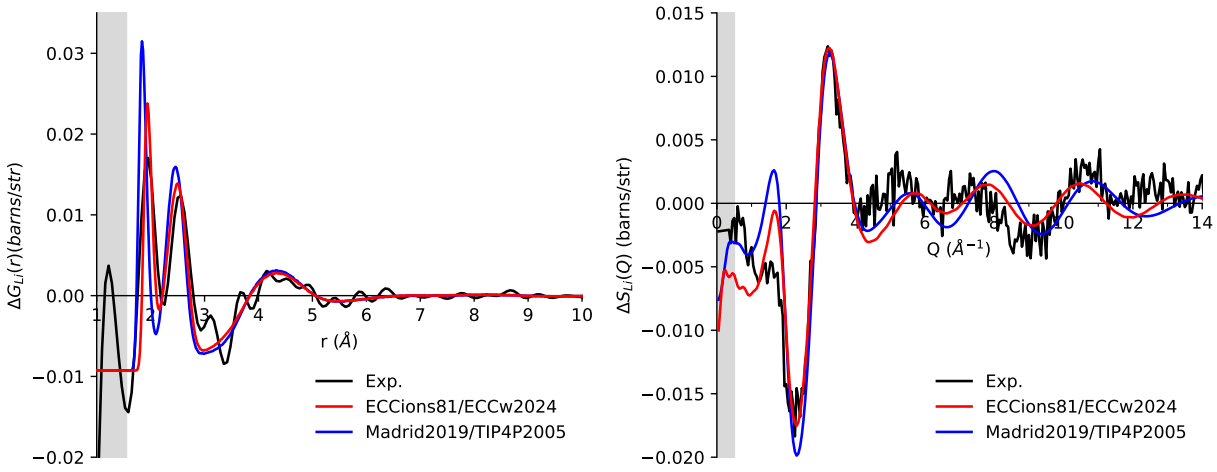

Figure 5: First-order difference functions $\Delta G_{Li}(r)$ (left) and $\Delta S_{Li}(Q)$ (right) for simulations of 3m LiCl solution using the ECCions81 model with the ECCw2024 water model (red) and the Madrid2019 ion model with the TIP4P/2005 water model (blue), and experimental data (black). Gray shading indicates regions where the experimental signal consists of only noise (in r-space) or falls outside the measurement range (in Q-space).

Lithium represents a special case among monovalent ions due to its small size, resulting

in a large charge density and, consequently, in a well-defined first coordination shell. The hydration structure of Li^+ was obtained in 3 m and 6 m LiCl solutions, with comparisons between simulation and experimental data shown in Figures 5 and S3. In r-space, both the ECCions81 and Madrid2019 models roughly reproduce the structure of the signals at both concentrations. Two closely spaced peaks represent the Li^+-O and Li^+-H correlations, respectively, while a third broader peak arises from a mixture of Li^+-O, Li^+-H, and Li^+-Cl correlations (Figures S2 and S4). The Madrid2019 model overestimates the Li^+-O and Li^+-H correlations, with the Li^+-O peak approximately 50% higher than the experimental value at 3 m and 100% higher at 6 m, indicating a tighter first hydration shell. In contrast, the ECCions81 model correctly lowers the Li^+-O and Li^+-H peaks. While the LiO peak still remains somewhat higher than the experimental value, the Li-H peak aligns closely with the experimental data. The difference between the two force fields arises from the larger σ_{LiO} in ECCions81 compared to Madrid2019 (Table S3), which also explains why the first peak of the ECCions81 model begins at a greater distance. Li-Cl pairing in ECCions81 leads to a reduction of the water density in the first hydration shell. In Q-space, ECCions81 shows better agreement with experimental data than Madrid2019, particularly in capturing the phase of the signal in the $Q > 6$ $Å^{-1}$ region at both 3 m and 6 m. Neither model fully captures the low-Q region for the 6 m solution, which reflects long-range structural information in r-space.

Sodium

For sodium, in order to emphasize the correlations between ions and water, the signal of 4m NaCl, $G_{\mathrm{Na}}(r)$, was subtracted from that of 4m KCl, $G_{\mathrm{K}}(r)$, or 4m LiCl, $G_{\mathrm{Li}}(r)$:

$$\begin{aligned} \Delta G_{\mathrm{NaK}}(r) &= G_{\mathrm{K}}(r) - G_{\mathrm{Na}}(r) \\ \Delta G_{\mathrm{NaLi}}(r) &= G_{\mathrm{Na}}(r) - G_{\mathrm{Li}}(r) \end{aligned} \tag{9}$$

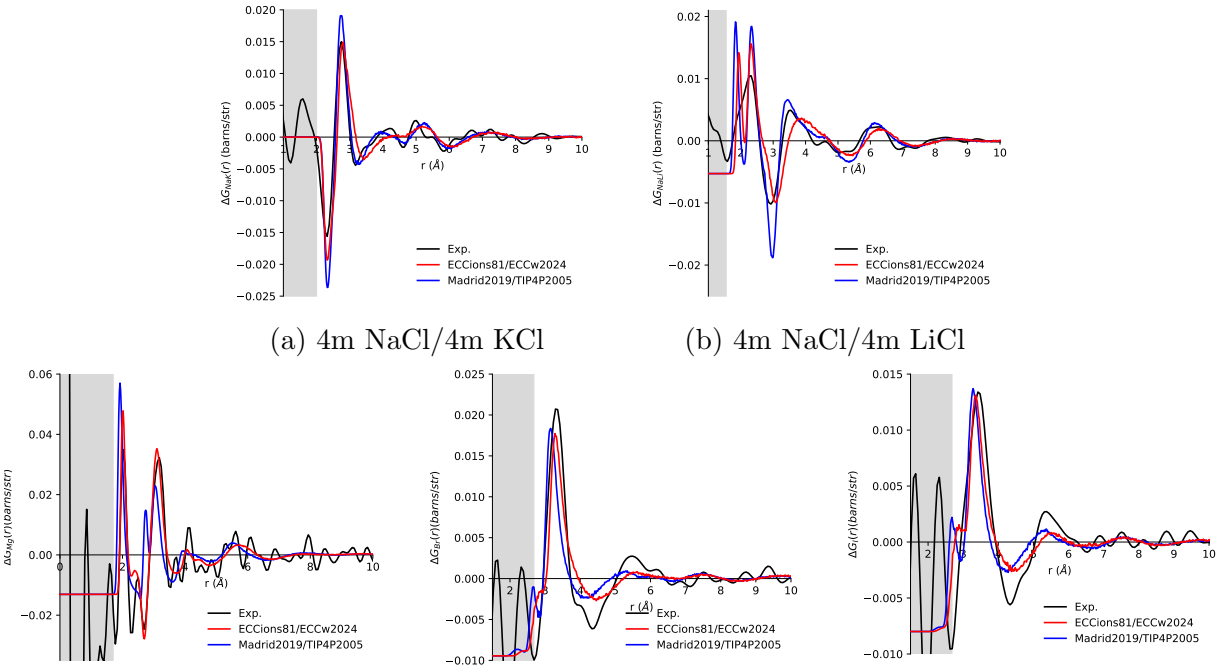

(a) 4m NaCl/4m KCl (b) 4m NaCl/4m LiCl

(c) 3m $MgCl_2$ (d) 4m KBr (e) 4m KI

Figure 6: First-order difference functions, $\Delta G_{MW}(r)$, for simulations of various cation or anion "M" in solutions using the ECCions81 model with ECCw2024 water (red), the Madrid2019 ion model with TIP4P/2005 water (blue), and experimental data (black). Panels (a) and (b) show $\Delta G_{MW}(r)$ for Na^+ in 4 m NaCl, subtracted by that of (a) K^+ in 4 m KCl and (b) Li^+ in 4 m LiCl. Panels (c)–(e) show $\Delta G_{MW}(r)$ for (c) Mg^{2+} in 3 m $MgCl_2$, (d) Br^- in 4 m KBr, and (e) I^- in 4 m KI.

. Figure 6 presents a comparison between simulations and neutron diffraction results for $\Delta G_{KNa}(r)$. In the corresponding Q-space data (Figure S9), a drop in the experimental baseline at 6 $Å^{-1}$ is observed due to the absence of 4 m KCl data beyond this point. Despite this, the available experimental data are sufficient to resolve the primary peaks, whose position and height are retained after Fourier transformation into r-space. In Q-space, both ECCions81 and Madrid2019 show phase differences relative to experiment but successfully capture the positions and intensities of the first two major peaks. In r-space, both models reproduce the main minima and maxima of the experimental signal. ECCions81 predicts a shallower Na–O minimum at 2.3 Å than Madrid2019, in better agreement with experiment. A broader first peak—arising from K–O and O–O correlations—is also observed in ECCions81 compared to the experimental data (for further discussion see SI).

Figure 6 also shows a comparison between the experimental $\Delta G_{\mathrm{NaLi}}(r)$ and results from simulations. ECCions81 and Madrid2019 both exhibit two distinct peaks between 1.8 and 2.7 Å, while the experimental signal shows a single, merged peak in this region. ECCions81 more accurately reproduces the experimental peak heights. Beyond 3 Å, however, ECCions81 shows a significant phase shift, whereas Madrid2019 aligns better with the experimental features. In Q-space, a similar trend is observed (Figure S11): ECCions81 deviates from experiment above 4 $Å^{-1}$, while Madrid2019 maintains consistent agreement across the full range. These discrepancies may partly result from inaccuracies in the O–O correlations of the LiCl reference system, which are not fully captured in the NDIS data (for further discussion see SI).

Magnesium

The hydration structures of Mg^{2+} in a solution of 3m $MgCl_2$ obtained from simulations using the ECCions81 and Madrid2019 models, compared with neutron diffraction data, are shown in Figure 6. To emphasize ion-water correlations, the total signal was subtracted by the O-O correlation in pure "null" water.

The ECCions81 model demonstrates better agreement with the experimental signal than the Madrid2019 model. Specifically, the ECCions81 model accurately reproduces the position of the first peak at 2 Å corresponding to the correlation between Mg and O (Figure S14), although the peak height is slightly overestimated compared to the experimental data. In contrast, the Madrid2019 model shows a significantly higher peak with a 0.1 Å deviation in the peak position. Neither model captures the first minima at approximately 2.3 Å. A small peak at 2.4 Å, between the first two minimas, corresponding to Mg-Cl correslations was only observed in ECCions81, not seen in Madrid2019. Additionally, the ECCions81 model accurately reproduces the second minima at 2.6 Å which corresponds to O-O correlations, while the Madrid2019 model displays a high peak at this position. This indicates that the ECCions81 model more accurately captures the influence of Mg^{2+} and Cl^{-} ions on O-O interactions. For the second main peak at around 3 Å, the ECCions81 model matches both the height and position of the experimental data well, whereas the Madrid2019 model shows a slight deviation in position and a significantly lower peak height. In Q-space, the ECCions81 model also exhibits better agreement with the experimental signal compared to the Madrid2019 model. This is particularly evident at the first peak at 2.4 $Å^{-1}$ and in the range between 6 and 10 $Å^{-1}$, where the ECCions81 model demonstrates better phase matching.

It is important to note that the water exchange rate in the first hydration shell of Mg^{2+} is very low—on the order of milliseconds for a single exchange event. Given the limited simulation timescales used during the optimization, it is clear that the sampling is insufficient to fully capture such slow exchange dynamics. Since all simulations, including those using the Madrid2019 parameters, began from the same initial structure but ultimately stabilized in different configurations, we assume that the system relaxes into a locally stable structure within the sampled timescale. However, this outcome should be interpreted with caution due to potential undersampling effects.

Chloride

Chloride is the anion present in all the solutions discussed above. This makes the Cl^-–water interaction a critical anchor point in developing the ECCion81 model. While detailed structural data are only available from NDIS measurements on a 6m LiCl solution, this dataset serves as a valuable benchmark for directly optimizing the Cl^-–water interaction.

Figure 7 compares the simulation results of the first-order difference functions in r-space and Q-space for Cl^- with NDIS data. While r-space and Q-space representations contain in principle the same information, they emphasize different aspects. Namely, Q-space highlights peak positions related to phasing, whereas r-space facilitates interpretation of peak heights.

In r-space, both ECCions81 and Madrid2019 models capture the first and second peaks, corresponding to the first and second solvation shells, which are clearly separated by a deep minimum at 2.8 Å. However, the Madrid2019 model significantly overestimates the height of the first peak, representing the correlations between Cl^- and hydrogen in water (Figure S5b). Additionally, the phases of the first and second peaks in Madrid2019 begin and end at shorter distances than those observed experimentally, indicating a tighter hydration shell for Cl^- compared to experiment.

In contrast, ECCions81 shows a smaller first peak, partly due to the presence of Li–Cl contact ion pairs (CIPs) within the first hydration shell (Figure S5a), with a CIP value of 0.43 (Table 2). This pairing reduces the water density around Cl^- in the first hydration shell. In Madrid2019, such pairing is deliberately avoided, resulting in a CIP value of zero. The ECC model also better than Madrid2019 matches the phase of the second peak, which includes contributions from the first peaks of g_{ClO} and the second peak of g_{ClH}. Both ECCions81 and Madrid2019 models fail to fully capture the second peak's height and position, while also displaying a deeper minimum between the first and second peaks. The Madrid2019 model achieves a comparable peak height but exhibits a narrower width and a shorter starting position, deviating from experimental observations. Conversely, ECCions81 accurately reproduces the position of the second peak but underestimates its height.

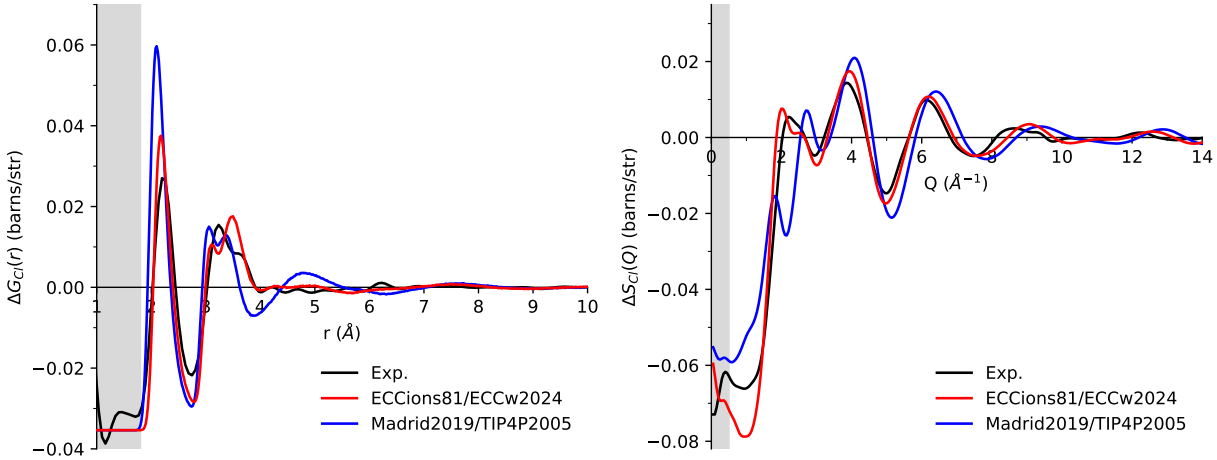

Figure 7: First-order difference functions $\Delta G_{Cl}(r)$ (left) and $\Delta S_{Cl}(Q)$ (right) for simulations of 6m LiCl solution using the ECCions81 model with the ECCw2024 water model (red) and the Madrid2019 ion model with the TIP4P/2005 water model (blue), and experimental data (black). Gray shading indicates regions where the experimental signal consists of only noise (in r-space) or falls outside the measurement range (in Q-space).

In Q-space, the Madrid2019 model fails to accurately capture the first peak between 2-3 $Å^{-1}$, where a single peak splits into two distinct peaks. In contrast, ECCions81 successfully reproduces the position of the first peak and provides a better match for peaks at higher Q values, with only a phase mismatch observed around 8 $Å^{-1}$. In the low Q region (< 2 $Å^{-1}$), neither model captures the signal effectively, which corresponds to long-range hydration structures hard to be observed in the r-space signal at distances greater than 4 Å.

Bromide

Similar to $MgCl_2$, the neutron diffraction data for KBr was processed by subtracting a weighted signal of O-O correlations in pure "null" water. The resulting data, along with those obtained from MD simulations using the ECCion81 and Madrid2019 ion models, are shown in Figure 6. In r-space, ECCions81 exhibits overall better agreement with the experimental signal, capturing the phase of peaks and valleys more accurately. In contrast, Madrid2019 predicts a shorter Br-O distance in the first hydration shell (Figure S16). However, both models fail to fully reproduce the amplitudes of all peaks and valleys.

The most notable difference between ECCion81 and Madrid2019 is the peak at 2.8 Å predicted by Madrid2019, which is absent in the experimental data and appears only as a small bump in the ECCions81 signal—indicating that ECCion81 provides a structure closer to the experimental one. As shown in Figure S16, this peak or bump originates from K-O correlations, which are partially canceled by differences in O-O correlations between pure water and the KBr solution (ΔG_{OO}). As discussed in Section Potassium Chloride, Madrid2019 overestimates K-O correlations. Here, it also exhibits larger ΔG_{OO}) compared to ECCions81, though these differences are insufficient to fully compensate for the overestimated K-O signal, leaving a noticeable peak at this position (for further details and discussion of Q-space data see SI).

Iodide

The results for KI solutions are similar to those for KBr. As shown in Figure 6, Madrid2019 again exhibits a peak at 2.8 Å in r-space, originating from K-O correlations, which are partially canceled by ΔG_{OO} (Figure S18). ECCion81, in contrast, shows a smaller bump at 2.9 Å from the same source and achieves a better phase match for the second peak. While both models capture the height of the first peak, neither accurately reproduces the width of the first peak, the amplitude of the first valley at 4.3 Å, or the second peak at 5.3 Å (for further details and discussion of Q-space data see SI).

Transferability

As emphasizes above, in parallel with structural neutron diffraction data the ECCion81 model was calibrated to reproduce also macroscopic physical properties—such as viscosity and density—in other chloride-containing solutions, ensuring broader transferability and consistency across diverse ionic environments.

The transferability of ECCions81 across water models was further tested using TIP4P2005. Despite having significantly different dielectric constants, ECCw2024 and TIP4P2005 exhibit

similar behavior for both density and viscosity (Figure S19). Consequently, the differences in our ion model performance between these two water frameworks are minimal, with deviations smaller than 1% (Tables S4 and S5). The only exception is the water self-diffusion coefficient, where neat water simulations with ECCw2024 yield D_{OW} values approximately 4% lower than those with TIP4P2005.[12] This difference propagates to electrolyte solutions at low concentrations (<1 m), where D_{OW} values calculated with ECCw2024 remain 5% lower than those obtained with TIP4P2005, as shown in Table S6. At higher concentrations (>3 m), nevertheless, D_{OW} values converge to similar values for both water models.

Similarly, the choice of water model, among good ones, has only a minor influence on the RDFs for all investigated cases. As an example of such a small effect, switching from ECCw2024 to TIP4P/2005 results in a slightly smaller second peak in the r-space data for Ca^{2+}, corresponding to the Ca–H correlation (Figure 8). In Q-space, the difference is barely noticeable in the 4–8$Å^{-1}$ range.

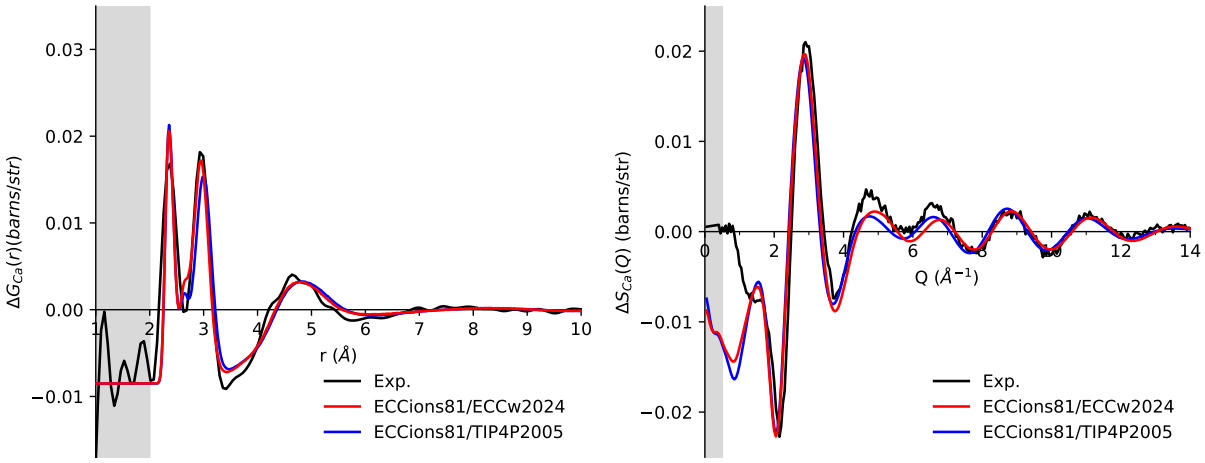

Figure 8: First-order difference functions $\Delta G_{Ca}(r)$ (left) and $\Delta S_{Ca}(Q)$ (right) for simulations of 4m $CaCl_2$ solution using the ECCions81 model with the ECCw2024 water model (red), and with the TIP4P/2005 water model (blue), and experimental data (black).

Conclusion

In this study, we developed a charge scaled ion force field, consistent with the a priori ECC-compatible ECCw2024 water model, for biologically relevant cations (Li^+, Na^+, K^+, Mg^{2+}, Ca^{2+}) and anions (Cl^-, Br^-, I^-) in concentrated aqueous solutions. The optimization process was conducted through an automated framework incorporating a LGP model to achieve global optimization across multiple target properties, including experimental neutron diffraction data, solution densities, and viscosities. The resulting ECCion81 parameterization was further validated against experimental data, comparing favorably to and in many aspects outperforming the hitherto best ion model, i.e., Madrid2019, also a charge scaled model.

The ECCion81 models, employing a scale factor of 0.81, demonstrated excellent agreement with experimental ion hydration structures across a wide range of concentrations. In particular, emphasizing correct cation-anion pairing significantly improved the ability of the model to reproduce neutron scattering data, in particular, the positions and heights of key peaks in r-space for Li^+, Na^+, K^+, Cl^-, Mg^{2+}, and Ca^{2+} ions. This performance surpassed that of the Madrid2019 model, which exhibits minimal ion pairing in the first hydration shell, except for K^+.

In terms of thermodynamic properties, the ECCion81 model successfully captures the concentration dependence of solution densities, showing comparable accuracy to Madrid2019, with the exception of $CaCl_2$, where the maximum deviation nevertheless did not exceed 4%. The ECCion81 model also exhibits high accuracy for viscosity and water self-diffusion coefficients, maintaining deviations typically below 10% even at high concentrations (up to 4m). In comparison, the Madrid2019 model displays significant deviations from experimental values at higher concentrations, particularly for viscosity and diffusion coefficients, where errors reached up to 60% in some cases.

Nevertheless, certain limitations of the ECCion81 model have been identified. Variations in the first-order difference function between 4m NaCl and 4m LiCl suggest that, while the ECC Li^+ model accurately captures ion–solvent correlations, it fails to accurately reproduce

changes in O–O correlations induced by Li^+. Additionally, a preliminary calculation of Na^+ solubility using the Kirkwood–Buff method[30] yielded a value of only about 1 m, significantly lower than the experimental value of 6.1 m. This discrepancy points to potentially overly too strong ion pairing in the first hydration shell, possibly due to overfitting to NDIS data. This issue may be partially addressed by adopting a less steep short-range potential, such as a Buckingham potential or a machine learning potential. These potentials should produce more realistic structural features without relying on artificially too strong ion pairing. The resulting RDFs from such improved potentials may then serve as more suitable references for re-optimizing the Lennard-Jones parameters.

Finally note that the ECC-fully consistent scaling factor for a water model with a dielectric constant around 45 is approximately 0.75, whereas the optimal value obtained in this work was 0.81. This is primarily due to the relatively high emphasis in the parameterization process on ion pairing, where we have shown previously that the dielectric screening is slightly attenuated for ions at close contact. At the same time, this represents a certain mismatch between the scaling factor and the dielectric constant of the water model. This indicates a future need to identify a fully consistent combination of the scaling factor and the dielectric constant of the water model. While our study shows robust behavior of water and ion models across a relatively broad range of dielectric constants and scaling factors, preliminary results, which form basis for our future work, point to an optimal choice of scaling charges by 0.8 in water with a dielectric constant of about 50-55.

Acknowledgement

P.J. acknowledges support from an ERC Advanced Grant (grant agreement no. 101095957).

References

(1) Leontyev, I. V.; Stuchebrukhov, A. A. Electronic Continuum Model for Molecular Dynamics Simulations of Biological Molecules. *6*, 1498–1508, Publisher: American Chemical Society.

(2) Leontyev, I.; Stuchebrukhov, A. Accounting for electronic polarization in non-polarizable force fields. *13*, 2613–2626, Publisher: Royal Society of Chemistry.

(3) Kirby, B. J.; Jungwirth, P. Charge Scaling Manifesto: A Way of Reconciling the Inherently Macroscopic and Microscopic Natures of Molecular Simulations. *10*, 7531–7536, Publisher: American Chemical Society.

(4) Duboué-Dijon, E.; Javanainen, M.; Delcroix, P.; Jungwirth, P.; Martinez-Seara, H. A practical guide to biologically relevant molecular simulations with charge scaling for electronic polarization. *153*, 050901, Publisher: American Institute of Physics.

(5) Kohagen, M.; Mason, P. E.; Jungwirth, P. Accurate Description of Calcium Solvation in Concentrated Aqueous Solutions. *118*, 7902–7909, Publisher: American Chemical Society.

(6) Mason, P. E.; Ansell, S.; Neilson, G. W.; Rempe, S. B. Neutron Scattering Studies of the Hydration Structure of Li+. *119*, 2003–2009, Publisher: American Chemical Society.

(7) Duboué-Dijon, E.; Mason, P. E.; Fischer, H. E.; Jungwirth, P. Hydration and Ion Pairing in Aqueous Mg^{2+} and Zn^{2+} Solutions: Force-Field Description Aided by Neutron Scattering Experiments and Ab Initio Molecular Dynamics Simulations. *122*, 3296–3306, Publisher: American Chemical Society.

(8) Martinek, T.; Duboué-Dijon, E.; Timr, S.; Mason, P. E.; Baxová, K.; Fischer, H. E.; Schmidt, B.; Pluhařová, E.; Jungwirth, P. Calcium ions in aqueous solutions: Accurate

force field description aided by ab initio molecular dynamics and neutron scattering. *148*, 222813, Publisher: American Institute of Physics.

(9) Berendsen, H. J. C.; Postma, J. P. M.; van Gunsteren, W. F.; Hermans, J. In *Intermolecular Forces: Proceedings of the Fourteenth Jerusalem Symposium on Quantum Chemistry and Biochemistry Held in Jerusalem, Israel, April 13–16, 1981*; Pullman, B., Ed.; Springer Netherlands, pp 331–342.

(10) Jorgensen, W. L.; Chandrasekhar, J.; Madura, J. D.; Impey, R. W.; Klein, M. L. Comparison of simple potential functions for simulating liquid water. *79*, 926–935.

(11) Abascal, J. L. F.; Vega, C. A general purpose model for the condensed phases of water: TIP4P/2005. *123*, 234505.

(12) Cruces Chamorro, V.; Jungwirth, P.; Martinez-Seara, H. Building Water Models Compatible with Charge Scaling Molecular Dynamics. *15*, 2922–2928, Publisher: American Chemical Society.

(13) Zeron, I. M.; Abascal, J. L. F.; Vega, C. A force field of Li^+, Na^+, K^+, Mg^{2+}, Ca^{2+}, Cl^-, and SO_4^{2-} in aqueous solution based on the TIP4P/2005 water model and scaled charges for the ions. *151*, 134504.

(14) Nencini, R.; Tempra, C.; Biriukov, D.; Riopedre-Fernandez, M.; Cruces Chamorro, V.; Polák, J.; Mason, P. E.; Ondo, D.; Heyda, J.; Ollila, O. H. S.; Jungwirth, P.; Javanainen, M.; Martinez-Seara, H. Effective Inclusion of Electronic Polarization Improves the Description of Electrostatic Interactions: The prosECCo75 Biomolecular Force Field. Publisher: American Chemical Society.

(15) Shanks, B. L.; Sullivan, H. W.; Shazed, A. R.; Hoepfner, M. P. Accelerated Bayesian Inference for Molecular Simulations using Local Gaussian Process Surrogate Models. *20*, 3798–3808, Publisher: American Chemical Society.

(16) Pluhařová, E.; Fischer, H. E.; Mason, P. E.; Jungwirth, P. Hydration of the chloride ion in concentrated aqueous solutions using neutron scattering and molecular dynamics. *112*, 1230–1240, Publisher: Taylor & Francis _eprint: https://doi.org/10.1080/00268976.2013.875231.

(17) Sindt, J. O.; Alexander, A. J.; Camp, P. J. Structure and Dynamics of Potassium Chloride in Aqueous Solution. *118*, 9404–9413.

(18) Badyal, Y. S.; Barnes, A. C.; Cuello, G. J.; Simonson, J. M. Understanding the Effects of Concentration on the Solvation Structure of Ca2+ in Aqueous Solution. II: Insights into Longer Range Order from Neutron Diffraction Isotope Substitution. *108*, 11819–11827, Publisher: American Chemical Society.

(19) Kohagen, M.; Mason, P. E.; Jungwirth, P. Accounting for Electronic Polarization Effects in Aqueous Sodium Chloride via Molecular Dynamics Aided by Neutron Scattering. *120*, 1454–1460, Publisher: American Chemical Society.

(20) Mason, P. E.; Ansell, S.; Neilson, G. W. Neutron diffraction studies of electrolytes in null water: a direct determination of the first hydration zone of ions. *Journal of Physics: Condensed Matter* **2006**, *18*, 8437.

(21) Abraham, M. J.; Murtola, T.; Schulz, R.; Páll, S.; Smith, J. C.; Hess, B.; Lindahl, E. GROMACS: High performance molecular simulations through multi-level parallelism from laptops to supercomputers. *1-2*, 19–25.

(22) Hoover, W. G. Canonical dynamics: Equilibrium phase-space distributions. *31*, 1695–1697.

(23) Parrinello, M.; Rahman, A. Polymorphic transitions in single crystals: A new molecular dynamics method. *52*, 7182–7190, Publisher: American Institute of Physics.

(24) Essmann, U.; Perera, L.; Berkowitz, M. L.; Darden, T.; Lee, H.; Pedersen, L. G. A smooth particle mesh Ewald method. *103*, 8577–8593, Publisher: American Institute of Physics.

(25) Hess, B. Determining the shear viscosity of model liquids from molecular dynamics simulations. *116*, 209–217.

(26) Maginn, E. J.; Messerly, R. A.; Carlson, D. J.; Roe, D. R.; Elliot, J. R. Best Practices for Computing Transport Properties 1. Self-Diffusivity and Viscosity from Equilibrium Molecular Dynamics [Article v1.0]. *1*, 6324–6324, Number: 1.

(27) Yeh, I.-C.; Hummer, G. System-Size Dependence of Diffusion Coefficients and Viscosities from Molecular Dynamics Simulations with Periodic Boundary Conditions. *108*, 15873–15879, Publisher: American Chemical Society.

(28) Kostal, V.; Jungwirth, P.; Martinez-Seara, H. Nonaqueous Ion Pairing Exemplifies the Case for Including Electronic Polarization in Molecular Dynamics Simulations. *14*, 8691–8696, Publisher: American Chemical Society.

(29) Hui, C.; de Vries, R.; Kopec, W.; de Groot, B. L. Effective polarization in potassium channel simulations: Ion conductance, occupancy, voltage response, and selectivity. `https://www.pnas.org/doi/10.1073/pnas.2423866122`, Publisher: Proceedings of the National Academy of Sciences.

(30) Chattopadhyay, A.; Mandalaparthy, V.; van der Vegt, N. F. A. Determination of aqueous solubility of NaCl in molecular dynamics simulation using the Kirkwood–Buff method. *162*, 174116.

TOC Graphic